# Difference between fracture of thin brittle sheets and two-dimensional fracture

J. A. Åström*
*CSC–IT Center for Science, P.O. Box 405, FIN-02101 Esbo, Finland*
(Received 17 June 2009; revised manuscript received 4 August 2009; published 19 October 2009)

Recently there has been some suggestions that fragmentation of thin brittle sheets is qualitatively different from pure two-dimensional fragmentation. The obvious reason for such a discrepancy is the possibility of the sheet to deform out of plane. There is a generic crack-branching mechanism that creates power-law fragment size distribution in the small fragment range for two-dimensional (2D) and three-dimensional bulk fragmentation with the power exponent $(2D-1)/D$. For thin sheets, the power exponent seems to be close to 1.2 which differs from the $D=2$ exponent 1.5. In order to make a distinct separation between sheet and 2D fragmentation, high-resolution fragment size distributions are required for fragmentation models with minimal differencies other than dimensionality. Here a very efficient numerical model which can be switched from 2D fragmentation to out-of-plane sheet fragmentation with minimal changes is used to produce high-resolution fragment size distribution for the two cases. The model results cast some doubt on the existence of separate universality classes for sheet and 2D fragmentation.

DOI: 10.1103/PhysRevE.80.046113 PACS number(s): 62.20.mm, 46.50.+a, 64.60.−i

One of the very early attempts to model fragmentation processes and to explain fragment size distributions (FSDs) was conducted in the 1940s by Mott [1–3]. He blasted thick shells and collected the fragments to form FSDs. Mott also made attempts to explain the distribution functions by comparison with a one-dimensional Poisson process and a two-dimensional (2D) random construction of horizontal and vertical lines dividing a plane into pieces [4]. The line construction results in a cumulative FSD, i.e., the relative number of fragments with size larger than area $S$, of the form $N(S) \propto \sqrt{S}K_1(\sqrt{S})$, where $K_1$ is a modified Bessel function. This form of $N(S)$ is fairly close to the more simple FSD of the one-dimensional (1D) Poisson process $N(S) \propto \exp(-\sqrt{S})$ [5].

Later Grady and Kipp [5] extended the line construction model to include several different set of rules for constructing the line grid. Obviously, the most realistic constructions are those that do not allow lines to intersect. These typically result in FSDs close to that of a two-dimensional Poisson process $N(S) \propto \exp(-S)$, which is different from the 1D Poisson process above.

The perhaps most well-known papers on fragmentation are those of Gilvarry [8] and of Gilvarry and Bergstrom [9]. Gilvarry derived a theoretical FSD under the assumption that uncorrelated flaws within the volume, on the surface and along the edges of existing fragments are activated in an uncorrelated fashion during fragmentation. The empirical Rossin-Rammler [10] and Gates-Gaudin-Schuhmann [11–13] FSDs and the experimental FSD of Gilvarry and Bergstrom are all consistent with the theoretical result of Gilvarry if it is assumed that edge flaws are dominant. The distribution of fragments with size between $S$ and $S+dS$ is then given by

$$n(S) \propto q(S)S^{-(d-1)/d} \exp(-S/S_0)dS, \qquad (1)$$

where $D$ is the Euclidean dimension, $S_0$ relates to the frequency of the Poisson process and $q(S)$ is the density of "*a priori*" fragments of size $S$. This parameter Gilvarry set to $q(S)=V_0/S$, where $V_0$ is the volume of the unbroken object.

Equation (1) seems to excellently explain numerous FSDs of fragmentation experiments and numerical simulations [14]. There are, however, some important unresolved issues of the Gilvarry theory. First, it is unclear when and how the *a priori* fragments, $q(S)=V_0/S$, are formed. Second, Gilvarry assumed that once flaws are activated they form smooth cracks. More recently it has been established that rapidly propagating cracks in brittle materials are not stable, but crack branching and crack tip splitting appear beyond some critical crack velocity [16]. Fragmentation cracks are obviously always fast, which means that such instabilities will destroy smooth crack surfaces and small fragments will be formed in "damage zones" along the paths of propagating cracks. These fragments are not included in the Gilvarry model and they will have a significant affect on the FSD in the small fragment range [15], which makes the validity of the model doubtful.

Inspired by the crack-branching mechanism it was rather recently proposed that the distribution of distances between initiated crack branches may explain the shape of FSDs in some cases. These distances have been found to have a log-normal distribution [17,18], which could then explain the appearance of log-normal FSDs. An important mechanism missing in such a model is that cracks, including crack branches, are attracted by a free surface. For example, the crack surface left behind by another crack. This means that a crack that is propagating beside another crack will turn toward it and they will merge. As the crack reaches the free surface the stress concentration at the crack tip vanish and the crack "dies." As increasing number of the crack branches merge with other branches the decreasing number of remaining daughter cracks will form increasingly larger fragments as they propagate further away from the mother crack expanding the damage zone around the crack. This will continue until all daughter cracks have merged with another crack or stopped as a result of stress relaxation.

A numerical model based on the crack-merging scenario

*astrom@csc.fi

 

was investigated by Inaoka and Takayasu [20,21]. The numerical FSDs were found to be consistent with the Gilvarry result $\gamma=\frac{3}{2}$ and $\gamma=\frac{5}{3}$ in 2D and three-dimensional (3D), respectively; i.e., $\gamma=\frac{2D-1}{D}$.

A theoretical proof that the crack-branching-merging scenario indeed leads to a power-law FSD with $\gamma-1=\frac{D-1}{D}$, can be found in Ref. [22].

The entire process with multiple unstable cracks producing branches which form damage zones with merging branches has been simulated numerically using first principle models in Refs. [23–25]. If the main cracks are initiated in an uncorrelated fashion they will divide the unfragmented sample according to a Poisson process, consistent with the Grady and Kipp model [5]. Then the entire FSD consist of a power law at small sizes with a cutoff determined by the width, $\lambda$, of the damage zones. For large fragments the FSD will have an exponential shape. The generic FSD for brittle fragmentation thus has the form

$$n(S) \propto (1-\beta_r)S^{-\gamma}\exp(-(2/\lambda)^D S) + \beta_r \exp(-S_0^{-1}(S^{1/D}+\lambda)^D), \quad (2)$$

where $\gamma=\frac{2D-1}{D}$, $S^{1/D}+\lambda$ is the reduced linear size of the Poisson-process fragments and $\beta_r$ determines the relative normalization of the two parts of the distribution.

Very recently [26,27] there has appeared reports that fragmentation of brittle thin sheets in a three dimensional space differs from two-dimensional fragmentation which produces FSDs with $\gamma=1.5$. For thin sheets the FSDs has been fitted with simple power laws, $n(S)\propto S^{-\alpha}$, with $\alpha\approx 1.2$. These results are also supported by earlier experiments [6,7]. This suggest that there may exist another universality class for fragmentation of thin sheets. An intuitive explanation [27] is that the difference stems from the possibility of out-of-plane deformations as thin sheets are fragmented. This is obviously forbidden for 2D fragmentation. However, the exact mechanism for the out-of-plane fragmentation and the derivation of the value 1.2 has remained unknown. The reported FSDs also typically have rather large fluctuations which would make weak deviations from a pure power law impossible to detect.

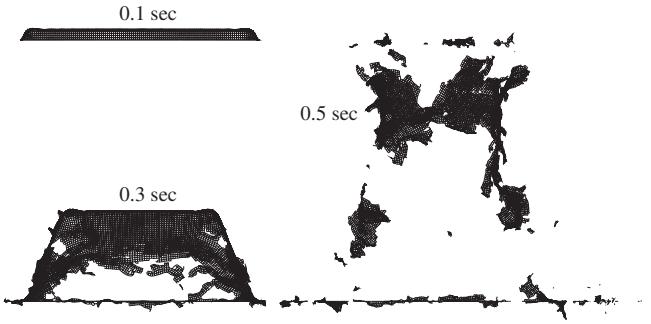


FIG. 1. A square lattice of mass points connected by breakable elastic beams. The lattice is anchored to a frame and fragmented by a vertical velocity pulse. The size of the lattice is $60\times 60$. The times of the snapshots are indicated.

Here, a discrete element model (DEM) of fragmentation is outlined which can, with minimal adjustments, simulate both 2D and sheets fragmentation. The model is designed to be numerically efficient in order to produce high-resolution FSDs which are used to investigate in detail the elusive difference between 2D and sheet fragmentation.

The DEM model consist of mass points connected by linear elastic beams [23]. The elastic energy of the beam model can be written as $(1/2)\mathbf{k}\vec{x}^2$, where $\vec{x}$ is the displacement vector containing translational and rotational displacements of two connected mass points. If $x_1$ and $x_7$ are the displacements of the two connected mass points along the axis of the beam that connects them, $(x_2,x_8)$ and $(x_3,x_9)$ the displacement pairs in the two perpendicular directions and $(x_4,x_{10})$, $(x_5,x_{11})$, and $(x_6,x_{12})$, the rotations of the mass points around the coordinate axis, The **K** matrix is given as

$$\begin{bmatrix}
\alpha & 0 & 0 & 0 & 0 & 0 & -\alpha & 0 & 0 & 0 & 0 & 0 \\
0 & \beta & 0 & 0 & 0 & \gamma & 0 & -\beta & 0 & 0 & 0 & \gamma \\
0 & 0 & \beta & 0 & -\gamma & 0 & 0 & 0 & -\beta & 0 & -\gamma & 0 \\
0 & 0 & 0 & \zeta & 0 & 0 & 0 & 0 & 0 & -\zeta & 0 & 0 \\
0 & 0 & -\gamma & 0 & \eta & 0 & 0 & 0 & \gamma & 0 & \omega & 0 \\
0 & \gamma & 0 & 0 & 0 & \eta & 0 & -\gamma & 0 & 0 & 0 & \omega \\
-\alpha & 0 & 0 & 0 & 0 & 0 & \alpha & 0 & 0 & 0 & 0 & 0 \\
0 & -\beta & 0 & 0 & 0 & -\gamma & 0 & \beta & 0 & 0 & 0 & -\gamma \\
0 & 0 & -\beta & 0 & \gamma & 0 & 0 & 0 & \beta & 0 & \gamma & 0 \\
0 & 0 & 0 & -\zeta & 0 & 0 & 0 & 0 & 0 & \zeta & 0 & 0 \\
0 & 0 & -\gamma & 0 & \omega & 0 & 0 & 0 & \gamma & 0 & \eta & 0 \\
0 & \gamma & 0 & 0 & 0 & \omega & 0 & -\gamma & 0 & 0 & 0 & \eta
\end{bmatrix},$$

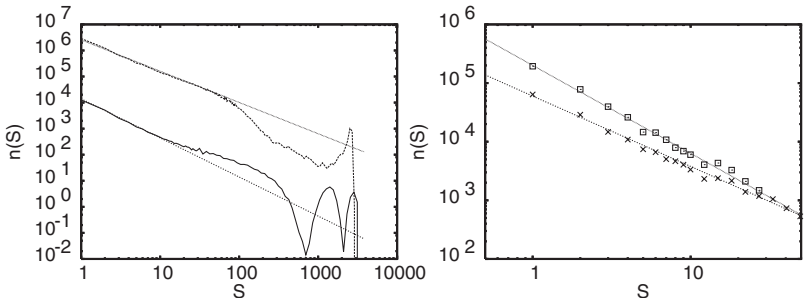


FIG. 2. Left: Simulated FSDs for 2D (lower curve) and sheet (upper curve) compared with power laws (straight lines) with $\alpha=1.5$ and $\alpha=1.2$, respectively. Right: similar data for fragment sizes in the range 1–20, in lattice units.

where $\alpha=\frac{EA}{L_s}$, $\beta=\frac{12EI}{L_s^3}$, $\gamma=\frac{6EI}{L_s^2}$, $\zeta=\frac{GI_r}{L_s}$, $\eta=\frac{4EI}{L_s}$, $\omega=\frac{2EI}{L_s}$, and $E$ is Young's modulus, $A$ is the cross-sectional area of a fiber, and $L_s$ is the length of a fiber segment. $I$ is the moment of inertia with respect to a cross-sectional symmetry axis (assumed to be similar in at least two directions). $I_r$ is the moment of inertia with respect to the center point of the cross section. It is given by $I_r=\int_0^r dA' r'^2$, where $r$ is the radius of the beam and $dA'$ is the differential cross-sectional area of an element. The torsion modulus is given by $GI_r/L$, where $G=E/2(1+\nu)$ is the shear modulus with $\nu$ being the Poisson ratio.

The equation of motion for a network of beams can be written as

$$\mathbf{M}\ddot{\vec{x}}+\mathbf{C}\dot{\vec{x}}+\mathbf{K}\vec{x}=0, \tag{3}$$

where $\mathbf{M}$ is the (diagonal) mass matrix, $\mathbf{C}$ the (diagonal) damping matrix, and $\mathbf{K}$ the stiffness matrix of the entire network which can be constructed by summing elements of $\mathbf{k}$ for beams connected to the same mass points, after appropriate rotations of coordinates. Equation (3) can be written in the discrete form

$$\left[\frac{\mathbf{M}}{\Delta t^2}+\frac{\mathbf{C}}{2\Delta t}\right]x(t+\Delta t)=\left[\frac{2\mathbf{M}}{\Delta t^2}-\mathbf{K}\right]x(t)-\left[\frac{\mathbf{M}}{\Delta t^2}-\frac{\mathbf{C}}{2\Delta t}\right]x(t-\Delta t), \tag{4}$$

where $t$ is time and $\delta t$ is the time incremental.

The discrete form of the beam model (Eq. (4)) is easily implemented on a computer and when (time and space-dependent) boundary conditions and $x(t=0)$ is defined, the time development $x(t)$ can unambiguously be calculated.

For most fragmentation simulations there is further a need to determine a fracture criterion. If a Lennard-Jones type of potential model is used there is no such need since the attractive force between mass points vanish continuously. For other models the fracture criterion must be defined explicitly.

Choosing a proper fracture criterion is far from trivial. The "classical" fracture criterion of Tresca, von Mises, Mohr-Coulomb and the maximum normal (i.e., hydrostatic pressure) stress criterion can all be unified in a simple 'elliptical' stress criterion [19]. This criterion states that a material under tension fails at locations where

$$\frac{\sigma^2}{\sigma_0^2}+\frac{\tau^2}{\tau_0^2}\geq 1, \tag{5}$$

in which $\sigma$ is the normal stress and $\tau$ is shear stress. $\sigma_0$ and $\tau_0$ are material dependent constant.

Because both shear and normal stresses are easily defined for beams it is straight forward to implement this fracture criterion in the beam model. A fracture limit can either be defined for every beam separately or as a limit on the average stress over several beams. For a single beam, $\sigma$ is just the stress along the axis of the beam and shear $\tau$ is the off-axis stress. For several beams (e.g., for all beams connected to a single mass point) the average stress tensor can be divided in a traceless and a diagonal part which then defines local normal stress and shear, respectively. Here we use a fracture criterion for every beam separately. The constants in Eq. (5) are chosen such that fracture through normal stress dominates.

In the simulations, we use a square lattice which for sheet fragmentation is anchored to a frame. At $t=0$ a rapid velocity impulse is given to all mass points in the vertical direction (Fig. 1). For 2D fragmentation the impulse is given as an in-plane expansion pulse.

Fragments are defined as unbroken lattice unit squares at the end of a simulation. The size of a fragment is defined as the number of such squares that are held together as an unbroken piece.

Figure 1 shows snapshots taken from the side of a sheet during fragmentation. The size of the lattice is $60\times 60$. The times of the snapshots are indicated. In order to produce

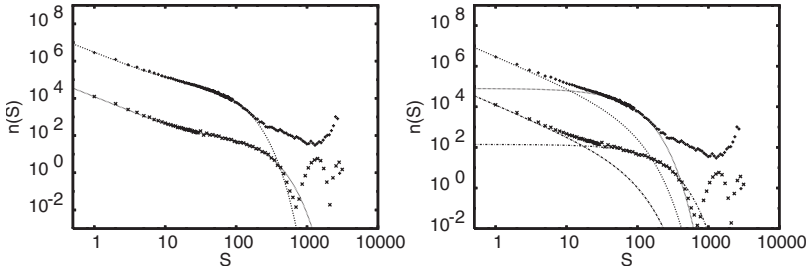


FIG. 3. The same data as in Fig. 2 compared to the FSD given by Eq. (2). Left: the full Eq. (2) fitted to the data. Right: The two parts of Eq. (2) as separate curves.

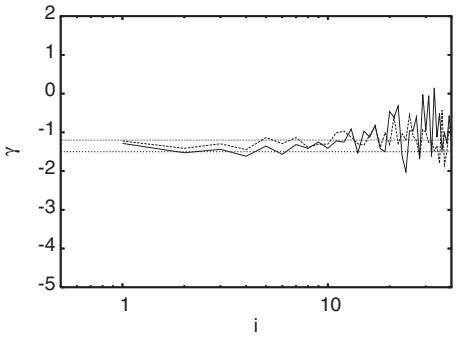


FIG. 4. The logarithmic slope of the distribution functions for pairs of fragment sizes $i$ and $i+1$. The horizontal lines are the slopes 1.2 and 1.5. The broken line represent sheet fragmentation and the full line 2D fragmentation.

high-resolution FSDs $10^3-10^4$ sheets were fragmented to create a single distribution.

Figure 2 displays simulated FSDs for 2D and sheet fragmentation. The simulation data is compared to power laws, $n(S) \propto S^{-\alpha}$, with $\alpha=1.5$ and $\alpha=1.2$, respectively. This figure confirms that the present model is able to reproduce the earlier reported results.

At this point it would be easy, based in Fig. 2, to draw the conclusion that there is indeed a different universality class for sheet fragmentation. If, however, Eq. (2) is fitted to the same distributions, the match is equally good. The scale on the $y$ axis is the only fetch factor used in Fig. 2. In Fig. 3 the $y$ scale is set separately for the two components of Eq. (2) and the cutoff size $S_0$ is fitted.

In order to investigate in more detail the logarithmic slope, i.e., the exponents $\gamma$ or $\alpha$, of the distribution functions in the small fragment range, the slope was calculated separately for every pair of fragments of size $i$ and $i+1$. The result is displayed in Fig. 4 and the values are given in Table I.

As can be seen from Fig. 4 and Table I the logarithmic slopes follows a rather similar trend for both 2D and sheet fragmentation. For the very smallest fragments (slope between fragment size 1 and 2 in lattice units) both slopes are quite close to 1.2. For fragment sizes in the range of 2–7 the slopes are closer to 1.5 than to 1.2 in both cases. For larger fragments the slopes approaches again 1.2. This indicates that neither sheet nor 2D fragmentation display pure power-law FSDs and that the fitted power-law FSDs with $\alpha=1.2$ for sheet fragmentation and $\alpha=1.5$ for 2D fragmentation are only approximations. The difference in the fitted exponents rather reflect differencies in the variations in the logarithmic slopes of the FSDs.

TABLE I. The logarithmic slope, $\gamma$, of the FSDs for pairwise fragment sizes in the small fragment range. The results are given for sheet and 2D fragmentation separately. For the smallest size (1–2), the discrete nature of the model is bound to affect the result.

| | $\gamma$ | |
|---|---|---|
| Size | 2D | Sheet |
| 1–2 | 1.28 | 1.22 |
| 2–3 | 1.53 | 1.41 |
| 3–4 | 1.44 | 1.30 |
| 4–5 | 1.62 | 1.44 |
| 5–6 | 1.35 | 1.14 |
| 6–7 | 1.57 | 1.29 |

In summary, there are no conclusive evidence that there exist separate universality classes for sheet and 2D fragmentation. It is, however, extremely easy to draw such a conclusion based on simulation or experimental results as it is easy to fit, with a rather high accuracy, power laws to the data with power exponent close to 1.2 and 1.5, respectively. The model results presented here suggest that the differencies in the exponents only reflects different variations in slopes for the two cases and that neither of them are exact power laws. This makes the existence of two separate universality classes doubtful.

[1] N. F. Mott, Ministry of Supply, AC 3642, March 1943.
[2] N. F. Mott, Ministry of Supply, AC 4035, May 1943.
[3] N. F. Mott, Proc. R. Soc. London, Ser. A **189**, 300 (1947).
[4] N. F. Mott and E. H. Linfoot, Ministry of Supply, AC 3348, January 1943.
[5] D. E. Grady and M. E. Kipp, J. Appl. Phys. **58**, 1210 (1985).
[6] L. Oddershede, P. Dimon, and J. Bohr, Phys. Rev. Lett. **71**, 3107 (1993).
[7] A. Meibom and I. Balslev, Phys. Rev. Lett. **76**, 2492 (1996).
[8] J. J. Gilvarry, J. Appl. Phys. **32**, 391 (1961).
[9] J. J. Gilvarry and B. H. Bergstrom, J. Appl. Phys. **32**, 400 (1961).
[10] P. Rosin and E. Rammler, J. Inst. Fuel **7**, 29 (1933).
[11] A. O. Gates, Trans. Am. Inst. Min., Metall. Pet. Eng. **52**, 875 (1915).
[12] A. M. Gaudin, Trans. Am. Inst. Min., Metall. Pet. Eng. **73**, 253 (1926).
[13] R. Schuhmann, Trans. Am. Inst. Min., Metall. Pet. Eng., Tech paper 1189, Min. Tech. (1940).
[14] J. A. Åström, Adv. Phys. **55**, 247 (2006).
[15] J. A. Åström and J. Timonen, Phys. Rev. Lett. **78**, 3677 (1997).
[16] J. Fineberg and M. Marder, Phys. Rep. **313**, 1 (1999).
[17] A. Bershadskii, J. Phys. A **33**, 2179 (2000).
[18] A. Bershadskii, Eur. Phys. J. B **14**, 323 (2000).
[19] Z. F. Zhang and J. Eckert, Phys. Rev. Lett. **94**, 094301 (2005).
[20] H. Inaoka and H. Takayasu, Physica A **229**, 5 (1996).
[21] H. Inaoka, E. Toyosawa, and H. Takayasu, Phys. Rev. Lett. **78**, 3455 (1997).
[22] P. Kekäläinen, J. A. Åström, and J. Timonen, Phys. Rev. E **76**, 026112 (2007).
[23] J. A. Åström, M. Kellomäki, and J. Timonen, Phys. Rev. E **55**,

4757 (1997).
[24] J. A. Åström, R. P. Linna, J. Timonen, P. F. Møller, and L. Oddershede, Phys. Rev. E **70**, 026104 (2004).
[25] J. A. Åström, F. Ouchterlony, R. P. Linna, and J. Timonen, Phys. Rev. Lett. **92**, 245506 (2004).
[26] R. P. Linna, J. A. Åström, and J. Timonen, Phys. Rev. E **72**, 015601(R) (2005).
[27] F. Wittel, F. Kun, H. J. Herrmann, and B. H. Kröplin, Phys. Rev. Lett. **93**, 035504 (2004).